This is a preprint, the final version is subject to change, of the American Mineralogist (MSA)
Cite as Authors (Year) Title. American Mineralogist, in press.
(DOI will not work until issue is live.) DOI: http://dx.doi.org/10.2138/am-2017-6109

REVISION 1

Thermodynamic characterization of synthetic autunite

EWA A. DZIK[1], HAYLIE L. LOBECK[1], LEI ZHANG[1], AND PETER C. BURNS[1,2]

[1]Department of Civil and Environmental Engineering and Earth Sciences, University of Notre Dame, Notre Dame, Indiana 46556

[2]Department of Chemistry and Biochemistry, University of Notre Dame, Notre Dame, Indiana 46556

*pburns@nd.edu, 301 Stinson-Remick Hall, Notre Dame, Indiana, 46556

Phone Number: 574-631-7852

ABSTRACT

Autunite, $Ca[(UO_2)(PO_4)]_2(H_2O)_{11}$, is a common uranyl mineral found in oxidized portions of uranium deposits, as well as subsurface environments contaminated by uranium. Enthalpies of formation of autunite were obtained via high-temperature oxide melt calorimetry using a $3NaMo•4MoO_3$ solvent at 976 K. The synthetic analogue of autunite was prepared using slow mixing by diffusion into an aqueous barrier solution at room temperature. Prior to calorimetric measurements, the material was characterized using powder X-ray diffraction (PXRD), inductively coupled plasma optical emission spectrometry (ICP-OES), thermogravimetric analysis (TGA), and Raman spectroscopy,

to ensure purity. The calculated enthalpy of formation from binary oxides of autunite is -563.86 ± 21.68 kJ/mol; the enthalpy of formation from the elements is -8138.90 ± 21.79 kJ/mol. The measured drop solution enthalpy allowed calculation of the enthalpy of the reaction of dehydration of autunite to meta-autunite. The results demonstrate that autunite is a metastable phase and explain the observed rapid dehydration to meta-autunite, a lower hydrate, as well as the common occurrence of the latter mineral in Nature.

KEYWORDS

Autunite, calorimetry, uranium, enthalpy, thermodynamics, metaphase

1. INTRODUCTION

Autunite, $Ca[(UO_2)(PO_4)]_2(H_2O)_{11}$, forms spectacular tabular crystals at famous localities including Spokane Co. (Washington, USA) (Leo, 1960) and the Viseu District, Portugal (Cook, 2005). Large autunite crystals are prized by museums and collectors, although their dehydration is spontaneous in air and can reduce the clarity of the crystals. It is a relatively common mineral in the altered portions of uranium deposits where phosphorous and calcium are present in groundwater (Krivovichev and Plášil, 2013). Its role in limiting the migration of uranium away from a uranium deposit was documented at Koongara, Australia (Murakami et al., 1997). Autunite is also recognized as an important uranium-bearing phase in the contaminated subsurface of various sites related to the production of nuclear weapons, including Fernald (OH) (Buck et al., 1996) and Oak Ridge (TN) (Roh et al., 2000).

Locock and Burns determined the crystal structure of autunite using single crystal X-ray diffraction (Locock and Burns, 2003). Owing to its rapid dehydration in air, the crystallographic data was collected for a single crystal contained in its mother solution (Locock and Burns, 2003). Autunite is orthorhombic, space group *Pnma*, although the crystals are pseudo-tetragonal. The structure of autunite consists of anionic sheets of uranyl square bipyramids and phosphate tetrahedra that are linked to each other by sharing vertices, giving a structural unit with composition $[(UO_2)(PO_4)]^-$ (Burns, 2005; Burns et al., 1997); Ca and H_2O are located in the interlayer region. About 40 phosphate and arsenate minerals and inorganic compounds contain sheets with the autunite-type typology (Krivovichev and Plášil, 2013; Locock, 2007).

Most, or perhaps all, natural specimens available are dehydrated forms of autunite, known as meta-autunite. Autunite is unstable in air (Locock and Burns, 2003; Sowder et al., 1996; Takano, 1961) and will eventually dehydrate to form its lower hydrate. Here we specifically focus on the synthetic analogue of autunite, and determination of its thermochemical properties for the first time. Gorman-Lewis performed batch solubility experiments of autunite from under- and supersaturation, and determined its solubility product and the standard Gibbs energy (Gorman-Lewis et al., 2009). Karyakin (Karyakin et al., 1998) reported thermodynamic properties of anhydrous and intermediate hydrates of (meta)autunite obtained using an adiabatic calorimeter in HCl solvent. However, no enthalpy or entropy data have been published for autunite. We have measured drop solution enthalpies using high-temperature oxide melt calorimetry for autunite, and calculated its enthalpies of formation from oxides and elements. These values can be used to evaluate the long-term stability of autunite in geochemical models related to uranium

ore deposit genesis, the mobility of uranium in a contaminated subsurface, and a geologic repository for nuclear waste.

2. MATERIALS AND METHODS

2.1. Synthesis

Natural specimens of autunite typically lack the purity required for thorough determination of their thermodynamic data, as well as the specific hydration state because autunite is susceptible to partial dehydration. The simple apparatus used previously for synthesis of other uranyl mineral analogs (Dzik et al., in press) and employed in this study provides high quality and purity material that is easy to recover, as well as the substantial quantity of sample needed to perform full thermodynamic evaluation, preceded by thorough chemical characterization. Crystals of the synthetic analogue of autunite were obtained by the slow mixing of reactants by diffusion into an aqueous barrier solution at room temperature, as described in detail by (Dzik et al., in press). Saturated solutions of $UO_2(NO_3)_2 \cdot 6H_2O$ (IBI Labs) and aqueous 0.5 M H_3PO_4 (EMD, Spectrum) were diffused into an aqueous barrier solution containing 0.05 M $Ca(NO_3)_2$ (99.9%, Alfa-Aesar). All reagents, unless stated otherwise, were analytical grade.

2.2. Powder X-ray diffraction (PXRD)

PXRD measurements were done using a Bruker D8 Advance Davinci powder diffractometer ($CuK\alpha$ radiation, 40 kV and 40 mA), at room temperature over the 2θ range of 5-55° with a step size of 0.01° and a fixed counting time of 1s/step. The sample was gently ground using an agate mortar and pestle, to minimize preferred orientation of

93 crystals arising from their platy morphology. Ground powder was placed on a zero
94 background quartz slide that was rotated during the data collection. Autunite was
95 identified using the ICCD PDF-4+ software.
96
97 2.3. Chemical analysis
98 Uranium, phosphorous, and calcium contents were obtained using a Perkin Elmer
99 Optima 8000 inductively coupled plasma optical emission spectrophotometer (ICP-OES).
100 The sample was prepared for wet chemical analysis by dissolving ~25 mg of crystals in
101 concentrated (6M) HCl, and subsequent dilutions were made in 5% HNO_3. Calculated
102 concentrations of each element in the samples were based on calibration coefficients of
103 0.99% or higher.
104
105 2.4. Thermogravimetric analysis
106 The water content of autunite was measured using thermogravimetric analysis (TGA)
107 with subsequent differential scanning calorimetry (DSC) (Metler Toledo TGA-DCS1
108 instrument). About 10 mg of powdered sample was placed in an alumina crucible and
109 heated from room temperature to 800 °C, with a heating rate of 5 °C/min. The sample
110 holder was purged during the measurement using nitrogen gas at a flow rate of 80
111 mL/min. The water content was calculated using the mass loss resulting from heating of
112 the sample.
113
114 2.5. Raman spectroscopy

A Raman spectrum was obtained using a Bruker Sentinel system equipped with a fiber optic probe, thermoelectric cooled CCD detector, and a 785 nm, 200 mW laser power. A powdered sample of synthetic autunite was placed on a glass slide and mounted on the stage of the microscope with a video-assisted fiber probe, which is part of the Raman setup (McGrail et al., 2012). The minimum power required to acquire an adequate signal-to-noise ratio in the spectrum was used to minimize sample damage and dehydration. The spectrum was collected in the range of 80 to 3200 cm^{-1} for 15 s with 6 signal accumulations.

2.6. High-temperature oxide melt calorimetry

A high-temperature Setaram AlexSys calorimeter was used to obtain enthalpies of drop solution of autunite. The solvent was molten sodium molybdate ($3NaMo•4MoO_3$) at 976 K. The calorimeter was calibrated against the heat content of ~5 mg of Al_2O_3. The instrument, calorimetric experiment, and calorimeter calibration are described elsewhere in detail (Navrotsky, 1977; Navrotsky, 1997; Navrotsky, 2014; Shvareva et al., 2012). Silica crucibles were used in this study, as they were found to be as reliable as previously used platinum crucibles. A semi-micro balance was used to weight out about 5 mg of powdered autunite, and then the sample was hand pressed into pellets. High purity O_2 was used to remove any water in the headspace of the calorimetric setup, that would have resulted from the dissolution of autunite in the sodium molybdate solvent. Visual inspection of the molten solvent after the experiment confirmed complete dissolution of the samples. Eight drop solution experiments were performed, to ensure reproducibility of the measurements (Table 1). Errors associated with calorimetric analyses are reported

as two standard deviations of the mean, and are less than 5% of the reported values of drop solution enthalpies (Table 1).

3. RESULTS AND DISCUSSION

Room temperature synthesis by slow mixing of reagents via diffusion in an aqueous barrier solution resulted in formation of synthetic autunite within four days, although crystals were left to grow for 14 days. The synthesis produced well-developed platy crystals, ranging up to about 200 μm in size (Figure 1). Crystals of autunite resulting from the synthesis were recovered, filtered, washed with 18MΩ water, and air-dried. Because of the potential dehydration of autunite to meta-autunite, all of the chemical analyses, as well as the calorimetric measurements, were carried out within two weeks of harvesting the material from solution.

The powder X-ray diffraction pattern of synthetic autunite (Figure SI 1) contains sharp peaks consistent with previously reported PXRD patterns for autunite. No additional peaks are present that could be attributed to impurities or lower hydrates of autunite. Note that the perfect cleavage and platy morphology of the crystals under study resulted in preferred orientation, which is reflected in the intensities of the diffraction maxima.

ICP-OES analysis confirmed the chemical composition of synthetic autunite and that it is indistinguishable from natural specimens. Molar concentrations of calcium and phosphorous were normalized to one mole of uranium, and are 1.05 M and 1.75 M, respectively. TGA analysis to 800 °C revealed that the synthetic material contains 11 moles of water per formula unit (Figure SI 2). This is identical to the fully hydrated

autunite formula that resulted from the earlier crystal-structure analysis (Locock and Burns, 2003). The DSC curve to 800 °C shows four endothermic peaks at 50, 65, 90, and 150 °C (indicated by arrows in Figure SI 2), all of which are attributed to water loss. After the fourth water loss that ends by about 160 °C, dehydration proceeds in a continuous manner. Although we did not examine the dehydration products obtained in the TGA as part of the current study, it is interesting to note that the uranyl phosphate sheets in metatorbernite, which are chemically and topologically identical to those in autunite, undergo a substantial reconstruction upon heating above 138° (Stubbs et al., 2010). Results of the chemical and thermal analyses are in good agreement with the reported ideal stoichiometry of autunite with instrumental uncertainties taken into consideration.

The Raman spectrum of synthetic autunite (Figure 2) contains the characteristic bands of uranyl and phosphate, and closely matches the previously published Raman spectra of natural samples of autunite (Driscoll et al., 2014). The most intense mode is the uranyl symmetric stretching vibration ($v_1(UO_2)^{2+}$) at 830 cm^{-1}. The bending uranyl modes ($v_2(UO_2)^{2+}$) are at 194 and 286 cm^{-1}, and the asymmetric stretch ($v_3(UO_2)^{2+}$) is present around 864 cm^{-1}. The phosphate asymmetric stretching mode ($v_3(PO_4)^{3-}$) is represented by two peaks (989 and 1007 cm^{-1}), indicating loss of the tetrahedral symmetry of the phosphate unit (Driscoll et al., 2014). The expected phosphate symmetric stretching mode ($v_1(PO_4)^{3-}$), in the 930 to 950 cm^{-1} range, is absent. This has been reported previously (Frost and Weier, 2004), although the cause is unclear. Bands at 126 and 148 cm^{-1} are attributed to the lattice modes, as previously reported in the literature (Sanchez-Pastor et al., 2013).

The measured drop solution enthalpy, ΔH_{ds}, of autunite, as well as the reported values of ΔH_{ds} for UO_3, P_2O_5, and CaO in sodium molybdate at 976 K are listed in Table 2. Thermodynamic cycles were used to calculate enthalpies of formation from binary oxides and elements for autunite and are also presented in Table 2.

The enthalpy of drop solution of autunite, measured using high-temperature drop solution calorimetry, is 1103.00 ± 21.37 kJ/mol. The large exothermic heat effect and change of the solvent color from colorless to yellow indicate complete dissolution of autunite during the calorimetric experiment. Enthalpies of formation from oxides and elements for autunite were calculated using thermochemical cycles, and are listed in Table 2. The enthalpy of formation from oxides ($\Delta H_{f\text{-}ox}$ = -563.86 ± 21.68 kJ/mol) is negative, suggesting that autunite is stable relative to its binary oxides at 297 K. Although the entropy of the reaction of the oxides to form autunite is unknown, it is most likely close to zero, since there are no gasses evolved or consumed during the calorimetric experiment. Hence, the free energy of formation of autunite (ΔG_f) mainly depends on its enthalpy of formation.

Previous studies showed that autunite readily dehydrates to meta-autunite, and this is known to degrade the quality of museum specimens. The calculated enthalpy of formation from binary oxides ($\Delta H_{f\text{-}ox}$) of meta-autunite is strongly exothermic (-602.1 ± 16.8 kJ/mol) (Dzik et al., in press). This suggests that meta-autunite is more energetically favorable than autunite relative to UO_3, P_2O_5, CaO, and H_2O at room temperature. Using the new data presented herein, we calculate the enthalpy of the dehydration reaction of autunite to meta-autunite, using enthalpies of drop solution of autunite, meta-autunite (Dzik et al., in press), and water obtained using the same calorimetric techniques.

207

208 $Ca[(UO_2)(PO_4)]_2(H_2O)_{11\ (s,\ 298\ K)} \rightarrow Ca[(UO_2)(PO_4)]_2(H_2O)_{4.2\ (s,\ 298\ K)} + 6.8\ H_2O_{\ (l,\ 298\ K)}$

209

210 The enthalpy of this reaction is exothermic (-38.22 ± 37.85 kJ/mol), confirming that
211 autunite is metastable relative to its lower hydrate, meta-autunite, and indicating that the
212 dehydration should be spontaneous. This thermodynamic data indicates that dehydration
213 of autunite to meta-autunite is irreversible, as has been reported previously on the basis of
214 rehydration attempts (Locock and Burns, 2003; Sowder et al., 1996; Takano, 1961).

215

216 ## 4. IMPLICATIONS

217 Despite the importance of autunite in understanding the fate of uranium in
218 contaminated environments, as well as the geochemical transport of uranium in near-
219 surface environments, its thermodynamic properties have not been fully defined. This is
220 in part due to its rapid dehydration to meta-autunite. Using synthetically prepared and
221 well-characterized autunite, the heat effect of dissolution of material into a high-
222 temperature flux has been measured, which allowed calculation of the heat of formation
223 from the oxides and elements under standard conditions. Although autunite is found to be
224 more stable than the mechanical mixture of its constituent oxides at 298 K, the
225 thermodynamic data show that it is metastable relative to the lower hydrate, meta-
226 autunite. Thermodynamic data such as presented here is a prerequisite to thermodynamic
227 models of uranyl phosphate systems.

228

229

Acknowledgments

This work is supported by the Office of Basic Energy Sciences of the U.S. Department of Energy as part of the Materials Science of Actinides Energy Frontier Research Center (DE-SC0001089). The ICP-OES analyses were conducted at the Center for Environmental Science and Technology (CEST) at the University of Notre Dame. PXRD, TGA, Raman spectroscopy, and high-temperature calorimetry data were collected in the Materials Characterization Facility supported by the Center for Sustainable Energy at Notre Dame (ND Energy).

253 **References:**

254 Buck, E.C., Brown, N.R., and Dietz, N.L. (1996) Contaminant uranium phases and
255 leaching at the Fernald site in Ohio. Environmental Science & Technology, 30,
256 81-88.
257 Burns, P.C. (2005) U6+ minerals and inorganic compounds: Insights into an expanded
258 structural hierarchy of crystal structures. Canadian Mineralogist, 43, 1839-1894.
259 Burns, P.C., Ewing, R.C., and Hawthorne, F.C. (1997) The crystal chemistry of
260 hexavalent uranium: Polyhedron geometries, bond-valence parameters, and
261 polymerization of polyhedra. Canadian Mineralogist, 35, 1551-1570.
262 Cook, R.B. (2005) Connoisseur's Choice: Autunite, Daybreak Mine, Spokane County,
263 Washington. Rocks & Minerals, 80, 188-193.
264 Driscoll, R.J.P., Wolverson, D., Mitchels, J.M., Skelton, J.M., Parker, S.C., Molinari, M.,
265 Khan, I., Geeson, D., and Allen, G.C. (2014) A Raman spectroscopic study of
266 uranyl minerals from Cornwall, UK. Rsc Advances, 4, 59137-59149.
267 Dzik, E.A., Lobeck, H.L., Zhang, L., and Burns, P.C. (in press) Thermodynamic
268 properties of phosphate members of the meta-autunite group: a high-temperature
269 calorimetric study. Journal of Chemical Thermodynamics.
270 Frost, R.L., and Weier, M. (2004) Raman microscopy of autunite minerals at liquid
271 nitrogen temperature. Spectrochimica Acta Part a-Molecular and Biomolecular
272 Spectroscopy, 60, 2399-2409.
273 Gorman-Lewis, D., Shvareva, T., Kubatko, K.A., Burns, P.C., Wellman, D.M.,
274 McNamara, B., Szymanowski, J.E.S., Navrotsky, A., and Fein, J.B. (2009)
275 Thermodynamic Properties of Autunite, Uranyl Hydrogen Phosphate, and Uranyl
276 Orthophosphate from Solubility and Calorimetric Measurements. Environmental
277 Science & Technology, 43, 7416-7422.
278 Grenthe, I., Fuger, J., Konings, R.J., Lemire, R.J., Muller, A.B., Nguyen-Trung, C., and
279 Wanner, H. (1992) Chemical thermodynamics of uranium. North-Holland
280 Amsterdam.
281 Helean, K.B., Navrotsky, A., Vance, E.R., Carter, M.L., Ebbinghaus, B., Krikorian, O.,
282 Lian, J., Wang, L.M., and Catalano, J.G. (2002) Enthalpies of formation of Ce-
283 pyrochlore, Ca0.93Ce1.00Ti2.035O7.00, U-pyrochlore,
284 Ca1.46U0.234+U0.466+Ti1.85O7.00 and Gd-pyrochlore, Gd2Ti2O7: three
285 materials relevant to the proposed waste form for excess weapons plutonium.
286 Journal of Nuclear Materials, 303, 226-239.
287 Karyakin, N., Chernorukov, N., Suleimanov, E., Belova, Y.S., and Alimzhanov, M.
288 (1998) Thermochemistry of the AII $(BVUO_6)_2$. NH_2O compounds. Russian
289 journal of inorganic chemistry, 43, 1552-1556.
290 Krivovichev, S.V., and Plášil, J. (2013) Mineralogy and crystallography of uranium.
291 Uranium: From Cradle to Grave. Mineralogical Association of Canada Short
292 Courses, 43, 15-119.
293 Leo, G.W. (1960) Autunite from Mt. Spokane, Washington. Am. Mineralogist, 45.
294 Locock, A. (2007) Trends in actinide compounds with the autunite sheet-anion topology.
295 Proceedings of the Russian Mineralogical Society, 123, p. 115-137.
296 Locock, A.J., and Burns, P.C. (2003) The crystal structure of synthetic autunite, Ca
297 (UO2)(PO4) (2)(H2O)(11). American Mineralogist, 88, 240-244.

McGrail, B.T., Jouffret, L.J., Villa, E.M., and Burns, P.C. (2012) In-Situ Raman Spectroscopy Studies of Room-Temperature and Hydrothermal Reactions. MRS Spring Meeting, 1444, p. 281-288. Materials Research Soc, Sacramento, CA.

McHale, J.M., Navrotsky, A., and DiSalvo, F.J. (1999) Energetics of ternary nitride formation in the (Li,Ca)-(B,Al)-N system. Chemistry of Materials, 11, 1148-1152.

Murakami, T., Ohnuki, T., Isobe, H., and Sato, T. (1997) Mobility of uranium during weathering. American Mineralogist, 82, 888-899.

Navrotsky, A. (1977) Progress and new directions in high-temperature calorimetry. Physics and Chemistry of Minerals, 2, 89-104.

-. (1997) Progress and new directions in high temperature calorimetry revisited. Physics and Chemistry of Minerals, 24, 222-241.

-. (2014) Progress and New Directions in Calorimetry: A 2014 Perspective. Journal of the American Ceramic Society, 97, 3349-3359.

Robie, R.A., Hemingway, B.S., and Fisher, J.R. (1978) Thermodynamic properties of minerals and related substances at 298. 15 K and 1 bar (10/sup 5/pascals) pressure and at higher temperatures. Geological Survey, Washington, DC (USA).

Roh, Y., Lee, S.R., Choi, S.K., Elless, M.P., and Lee, S.Y. (2000) Physicochemical and mineralogical characterization of uranium-contaminated soils. Soil & Sediment Contamination, 9, 463-486.

Sanchez-Pastor, N., Pinto, A.J., Astilleros, J.M., Fernandez-Diaz, L., and Goncalves, M.A. (2013) Raman spectroscopic characterization of a synthetic, non-stoichiometric Cu-Ba uranyl phosphate. Spectrochimica Acta Part a-Molecular and Biomolecular Spectroscopy, 113, 196-202.

Shvareva, T.Y., Fein, J.B., and Navrotsky, A. (2012) Thermodynamic Properties of Uranyl Minerals: Constraints from Calorimetry and Solubility Measurements. Industrial & Engineering Chemistry Research, 51, 607-613.

Sowder, A.G., Clark, S.B., and Fjeld, R.A. (1996) The effect of silica and phosphate on the transformation of schoepite to becquerelite and other uranyl phases. Radiochimica Acta, 74, 45-49.

Stubbs, J.E., Post, J.E., Elbert, D.C., Heaney, P.J., and Veblen, D.R. (2010) Uranyl phosphate sheet reconstruction during dehydration of metatorbernite Cu(UO2)(2)(PO4)(2)center dot 8H(2)O. American Mineralogist, 95, 1132-1140.

Takano, Y. (1961) X-RAY STUDY OF AUTUNITE. American Mineralogist, 46, 812-822.

Ushakov, S.V., Navrotsky, A., Farmer, J.M., and Boatner, L.A. (2004) Thermochemistry of the alkali rare-earth double phosphates, A(3)RE(PO4)(2). Journal of Materials Research, 19, 2165-2175.

This is a preprint, the final version is subject to change, of the American Mineralogist (MSA)
Cite as Authors (Year) Title. American Mineralogist, in press.
(DOI will not work until issue is live.) DOI: http://dx.doi.org/10.2138/am-2017-6109

Figures and tables

Figure 1. Crystals of autunite resulting from the benchtop synthesis involving slow mixing of nutrients by diffusion into a barrier solution. PXRD indicates that the fine-grained material present in the specimen is also autunite.

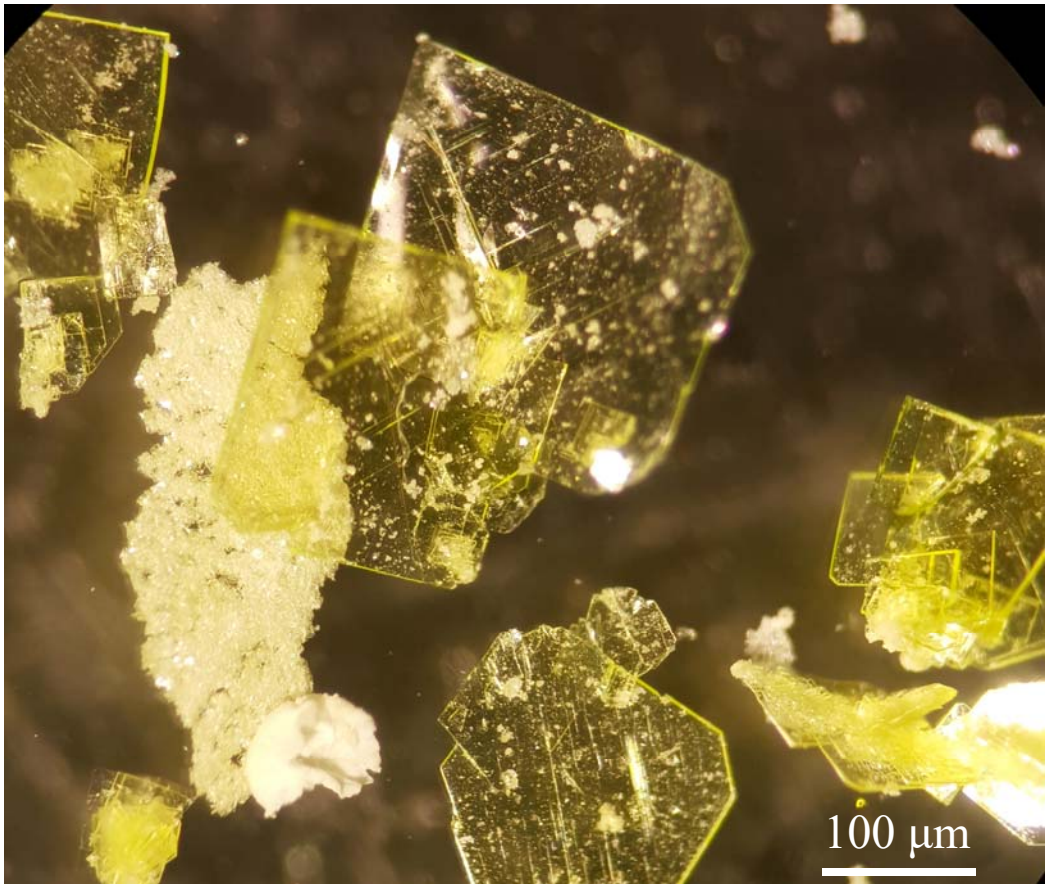

Figure 2. Raman spectrum of synthetic autunite. Major peaks are annotated, and all bands are listed in the supporting information file.

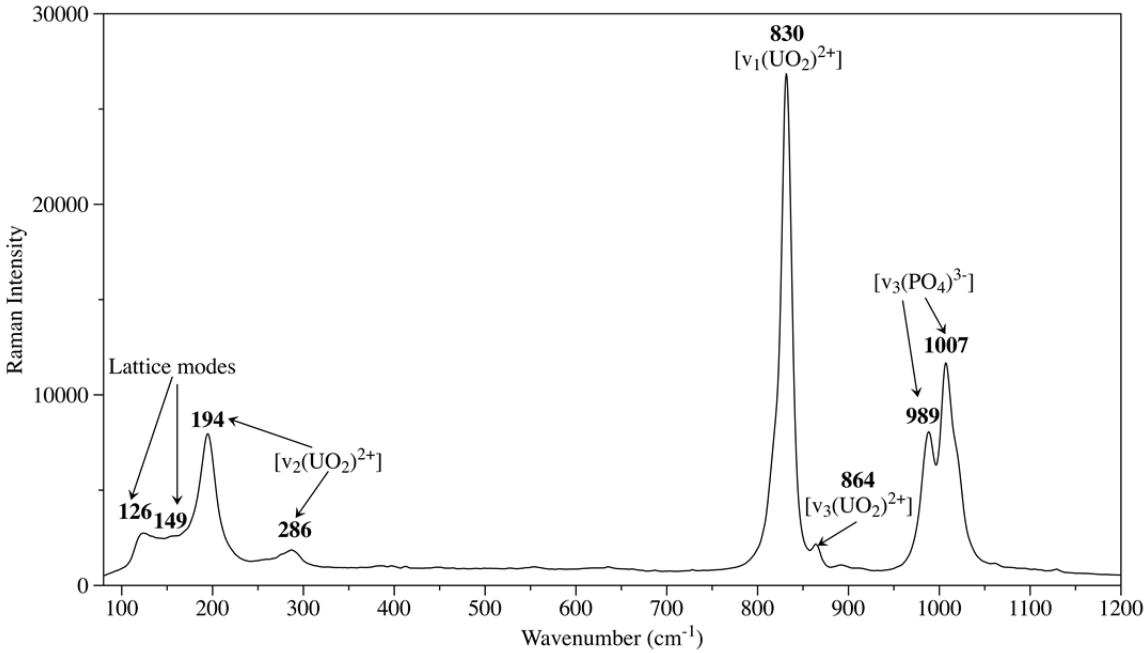

Table 1. Measured enthalpies of drop solution, ΔH_{ds} (kJ/mol), for autunite.

Mass (mg)	**ΔH_{ds} (kJ/mol)**
5.00	1105.61
4.64	1164.87
4.47	1040.31
4.29	1130.61
4.87	1138.61
5.24	1074.96
5.05	1080.11
4.40	1088.88
Average	1103.00
Error	21.37
Error (%)	1.97

405 Table 2. Thermochemical cycles for calculation of the enthalpies of formation from
406 oxides and elements at a constant pressure for autunite.
407

	Reaction		ΔH (kJ/mol)	Reference
1	ΔH_{ds} (autunite)	$Ca(UO_2)_2(PO_4)_2(H_2O)_{11}$ (s, 298K) = CaO (sln, 976K) + P_2O_5 (sln, 976K) + $2UO_3$ (sln, 976K) + $11H_2O$ (g, 976K)	1103.00 ± 21.37	This work
2	ΔH_{ds} (UO_3)	UO_3 (s, 298K) = UO_3 (sln, 976K)	9.49 ± 0.8	(Helean et al., 2002)
3	ΔH_{ds} (P_2O_5)	P_2O_5 (s, 298K) = P_2O_5 (sln, 976K)	-164.6 ± 0.85	(Ushakov et al., 2004)
4	ΔH_{hc} (H_2O)	H_2O (l, 298K) = H_2O (g, 976K)	69	(Robie et al., 1978)
5	ΔH_{ds} (CaO)	CaO (s, 298K) = CaO (sln, 976K)	-90.3 ± 1.8	(McHale et al., 1999)
6	ΔH_f^0 (UO_3)	U (s, 298K) + $3/2O_2$ (g, 298K) = UO_3 (s, 298K)	-1223.8 ± 0.8	(Grenthe et al., 1992)
7	ΔH_f^0 (P_2O_5)	2P (s, 298K) + $5/2O_2$ (g, 298K) = P_2O_5 (s, 298K)	-1504.9 ± 0.5	(Robie et al., 1978)
8	ΔH_f^0 (H_2O)	H_2 (g, 298K) + ½O_2 (g, 298K) = H_2O (l, 298K)	-285.8 ± 0.1	(Robie et al., 1978)
9	ΔHf^0 (CaO)	Ca (s, 298K) + ½O_2 (g, 298K) = CaO (s, 298K)	-635.1 ± 0.9	(Robie et al., 1978)
	$\Delta H_{f\text{-}ox}$ (autunite)	$-\Delta H_1 + \Delta H_5 + \Delta H_3 + 2\Delta H_2 + 11\Delta H_2O$	-563.86 ± 21.68	This work
		CaO (s, 298K) + P_2O_5 (s, 298K) + $2UO_3$ (s, 298K) + $11H_2O$ (g, 298K) = $Ca(UO_2)_2(PO_4)_2(H_2O)_{11}$ (s, 298K)		
	ΔH_f^0 (autunite)	$-\Delta H_1 + \Delta H_5 + \Delta H_3 + 2\Delta H_2 + 11\Delta H_2O + \Delta H_9 + \Delta H_7 + 2\Delta H_6 + 11\Delta H_8$	-8138.90 ± 21.79	This work
		Ca (s, 298K) + 2P (s, 298K) + 2U (s, 298K) + H_2 (g, 298K) + $23/2O_2$ (g, 298K) = $Ca(UO_2)_2(PO_4)_2(H_2O)_{11}$ (s, 298K)		

408